# Mechanism of Annexin I-Mediated Membrane Aggregation[†]

Eduard Bitto,[‡] Ming Li,[§] Aleksey M. Tikhonov,[§] Mark L. Schlossman,[‡,§] and Wonhwa Cho*,[‡]

*Departments of Chemistry (M/C 111) and Physics (M/C 273), University of Illinois at Chicago,
845 West Taylor Street, Chicago, Illinois 60607-7061*

*Received June 5, 2000; Revised Manuscript Received September 1, 2000*

ABSTRACT: It has been proposed that annexin I has two separate interaction sites that are involved in membrane binding and aggregation, respectively. To better understand the mechanism of annexin I-mediated membrane aggregation, we investigated the properties of the inducible secondary interaction site implicated in membrane aggregation. X-ray specular reflectivity measurements showed that the thickness of annexin I layer bound to the phospholipid monolayer was $31 \pm 2$ Å, indicating that annexin I binds membranes as a protein monomer or monolayer. Surface plasmon resonance measurements of annexin I, V, and mutants, which allowed evaluation of membrane aggregation activity of annexin I separately from its membrane binding, revealed direct correlation between the relative membrane aggregation activity and the relative affinity of the secondary interaction site for the secondary membrane. The secondary binding was driven primarily by hydrophobic interactions, unlike calcium-mediated electrostatic primary membrane binding. Chemical cross-linking of membrane-bound annexin I showed that a significant degree of lateral association of annexin I molecules precedes its membrane aggregation. Taken together, these results support a hypothetical model of annexin I-mediated membrane aggregation, in which a laterally aggregated monolayer of membrane-bound annexin I directly interacts with a secondary membrane via its induced hydrophobic interaction site.

Annexins are a family of structurally related eukaryotic proteins that reversibly bind the membrane containing anionic phospholipids in a $Ca^{2+}$-dependent manner (*1−3*). More than 20 different isoforms have been found in many organisms ranging from mammals to molds (*4*). Annexins have a conserved core made up of four highly helical domains of about 70 amino acids. The core domains harbor multiple calcium binding sites, which are all located on the convex side of the molecule (*5*). Annexins also contain an amino-terminal region that varies in length and amino acid sequence. The amino-terminal region has been implicated in regulating different functions of annexins (*1*, *6*). Although exact physiological functions of annexins are not fully understood, they have been implicated in a variety of processes, including regulation of membrane trafficking (*3*, *7*), modulation of blood coagulation (*8*, *9*), bone calcification (*10*, *11*), inhibition of phospholipase $A_2$ (*1*), modulation of cell signaling pathways (*12*, *13*), regulation of calcium homeostasis (*14*, *15*), and antiinflammatory actions of glucocorticoids (*16*).

Some annexins, including annexin I, II, IV, and VII, can promote membrane aggregation in vitro, which have led to a hypothesis that these annexins are involved in cellular endocytosis and exocytosis (*3*, *17*). However, the mechanisms by which annexins induce membrane aggregation have remained controversial. The cryo-electron microscopic imaging of vesicles aggregated by annexin II, annexin II-p11 heterotetrameric complex, and annexin I has pointed to the direct protein−protein interaction of the annexins bound to two separate membranes (*18*). However, ellipsometric measurements of annexin I−V chimera support the notion that an annexin molecule (or a monolayer of membrane-bound annexin molecules) simultaneously interacts with two separate membranes (*19*). Despite fundamental differences, these models share a common concept of two distinct interaction sites; a primary site for membrane binding and a secondary site for membrane aggregation. The primary membrane-binding site, which has been defined by extensive structural and mutational studies, coincides with the calcium-binding sites located on the convex surface of annexin molecules (*20−27*). Much less is known about the secondary interaction site, although it has been postulated to be on the opposite concave side of the annexin molecule that harbors the amino-terminal region (*19*, *28*, *29*).

To elucidate the mechanism of annexin I-mediated membrane aggregation and determine the properties of its secondary interaction site, we performed chemical cross-linking, X-ray specular reflectivity, and surface plasmon resonance (SPR) measurements. Results indicate that membrane-bound annexin I molecules laterally aggregate with their hydrophobic secondary interaction sites exposed, which then directly interact with the secondary membrane to induce membrane aggregation.

## MATERIALS AND METHODS

*Materials.* 1-Palmitoyl-2-oleoyl-*sn*-glycero-3-phospho-serine (POPS),[1] 1-palmitoyl-2-oleoyl-*sn*-glycero-3-phospho-choline (POPC), and 1-palmitoyl-2-oleoyl-*sn*-glycero-3-

* To whom correspondence should be addressed: Telephone: 312-996-4883; fax: 312-996-2183; e-mail: wcho@uic.edu.
‡ Department of Chemistry.
§ Department of Physics.

phosphoethanolamine (POPE) were purchased from Avanti Polar Lipids, Inc. (Alabaster, AL) and used without further purification. The expression and purification of annexins I and V and annexin mutants was performed as described previously (*24, 30, 31*).

*X-ray Reflectivity Measurements.* X-ray reflectivity was conducted at beamline X19C at the National Synchrotron Light Source (Brookhaven National Laboratory, USA) with a liquid surface spectrometer and measurement techniques described in detail elsewhere (*32*). In a typical experiment, 10 μL of 1 mM POPS/POPE/POPC (2:5:2 in mole ratio) in chloroform was added dropwise onto the surface of 10 mM HEPES-KOH buffer, pH 7.0, containing 0.1 M KCl and 1 mM $Ca^{2+}$ in a Langmuir trough (ca. 40 mL total volume). The resulting lipid monolayer was equilibrated for 30 min at 25 °C in a temperature-controlled aluminum container. After the surface pressure of the phospholipid monolayer was adjusted to 34 dyn/cm, 160 μg of annexin I or 500 μg of annexin V was injected into the subphase, and the system was equilibrated for another 2 h with intermittent stirring. The specular reflectivity is measured as a function of the wave vector transfer, $Q_z$, by varying the incident angle, α (measured from the plane of the water surface), and measuring the intensity of scattered X-rays at the reflected angle β where β = α (and the reflected X-rays are in the plane of incidence). In this case, the wave vector transfer of the reflected X-rays, $Q$, is solely in the z-direction normal to the water surface and is given by $Q_z = (4\pi/\lambda)\sin(\alpha)$, where λ = 1.54 ± 0.002 Å is the X-ray wavelength for these measurements. Typical data acquisition time for the single reflectivity curve was 6−8 h. No significant radiation damage was detected during the measurements, as indicated by the reproducibility of data after repeated (>2) measurements on the same sample.

The reflectivity, $R(Q_z)$, represents the scattered intensity normalized by the X-ray intensity immediately prior to the sample. To make the features of the reflectivity curve more evident, $R(Q_z)$ is divided by $R_F(Q_z)$, which is the Fresnel reflectivity predicted for an ideal, smooth, and flat interface (*33*). Deviations of the measured reflectivity, $R(Q_z)$, from the Fresnel reflectivity, $R_F(Q_z)$, reveal the presence of interfacial structure as a function of the position along the normal to the surface. In this case, the structure is due to the lipid monolayer supported on the water surface and to annexin and $Ca^{2+}$ ions adsorbed to the headgroup region of the lipid monolayer. Reflectivity data were analyzed using a general expression, derived from the first Born approximation for X-ray scattering, that relates the reflectivity to the electron density gradient normal to the interface, $(d\langle\rho_e(z)\rangle/dz)$ (averaged over the interfacial plane), and written as

$$\frac{R(Q_z)}{R_F(Q_z)} \cong \left|\frac{1}{\rho_{e,bulk}} \int dz \frac{d\langle\rho_e(z)\rangle}{dz} \exp(iQ_z z)\right|^2 \quad (1)$$

where $\rho_{e,bulk}$ is the electron density of the aqueous subphase

(*34*). The data from the lipid monolayer were analyzed by a two-slab model where one slab represents the average electron density in the acyl group region of the lipids and the other slab represents the electron density in the headgroup region. Addition of annexin required that a third slab be used to represent the additional electron density due to protein adsorbed onto the lipid monolayer. In the latter case of annexin adsorption, the model for the electron density gradient is given by

$$\frac{1}{\rho_{e,bulk}} \frac{d\langle\rho_e(z)\rangle}{dz} = (\rho_{acyl})(2\pi\sigma^2)^{-1/2}e^{-z^2/2\sigma^2} +$$
$$(\rho_{head} - \rho_{acyl})(2\pi\sigma^2)^{-1/2}e^{-[z - L_{acyl}]^2/2\sigma^2} +$$
$$(\rho_{ann} - \rho_{head})(2\pi\sigma^2)^{-1/2}e^{-[z - (L_{head} + L_{acyl})]^2/2\sigma^2} +$$
$$(\rho_w - \rho_{ann})(2\pi\sigma^2)^{-1/2}e^{-[z - (L_{ann} + L_{head} + L_{acyl})]^2/2\sigma^2} \quad (2)$$

where $L_{ann}$, $L_{head}$, $L_{acyl}$ are the thickness of the annexin, headgroup, and acyl group regions, respectively; $\rho_{ann}$, $\rho_{head}$, $\rho_{acyl}$ represent the average electron densities (normalized to the electron density of bulk water, $0.334\ e^-/Å^3$) of the annexin, headgroup, and acyl group regions, respectively; $\rho_w$ is the electron density of the water subphase (normalized to be equal to 1); and σ is the roughness of the surface determined primarily by capillary waves. The first term in eq 2 represents the interface between the vapor and the top of the lipid acyl group; the second term represents the interface between the bottom of the acyl group region and the headgroup region; the third term represents the interface between the bottom of the headgroup region and the annexin proteins; and the fourth term represents the interface between the bottom of the annexin proteins and the water subphase. The reflectivity calculated from eq 1 using the model given by eq 2 is then fit to the data to yield values for the fitting parameters: $L_{ann}$, $L_{head}$, $L_{acyl}$, $\rho_{ann}$, $\rho_{head}$, $\rho_{acyl}$, and σ. Some of these fitting parameters correspond to qualitative features of the data. For example, $L_{ann}$ is determined by the width of the first peak in the reflectivity and $\rho_{ann}$ is determined by the amplitude of that first peak.

*Surface Plasmon Resonance Measurements.* All SPR measurements were performed with a BIACORE X instrument and a Pioneer L1 sensor chip (BIACORE AB, Piscataway, NJ). The chip was coated with lipid by two sequential injections (90 and 40 μL) of 0.5 mM POPC/POPE/POPS (2:5:2 in mole ratio) LUV prepared in the flow buffer (10 mM HEPES-KOH, 0.1 M NaCl, 1 mM $Ca^{2+}$, pH 7.0). All measurements were performed at flow rate of 10 μL/min and 24 °C unless noted otherwise. The deposited lipid layer was washed with 30 μL of 10 mM NaOH at flow rate of 100 μL/min to ensure a stable surface. Lack of fluorescence signal in the flow buffer after rinsing the sensor chip coated with POPC/POPE/POPS vesicles incorporating 10 mM 5-carboxyfluorescien (Molecular Probes) indicated that the vesicles remained intact on the chip. Thirty microliters of freshly prepared annexin solutions (typically 100 nM) in the flow buffer was injected into the flow channel, and the association was monitored for 3 min. After unbound protein was allowed to be flushed away from the flow channel for 320 s, 30 μL of 0.5 mM POPC/POPE/POPS (2:5:2 in mole ratio) LUV in the flow buffer was injected. Kinetics of vesicle adsorption was followed for 3 min. The chip surface

was regenerated after each measurement by injections of 30 $\mu$L of 40 mM CHAPS and 30 $\mu$L of 10 mM octylglucoside. The salt dependence of vesicle adsorption was measured by the similar protocol with the following modifications. The lipid coating of chip was performed with vesicles prepared in the flow buffer containing 0.2 M NaCl instead of 0.1 M NaCl. The concentration of annexin solutions used for primary protein binding was adjusted to 10 nM instead of 100 nM. Phospholipid vesicles were freshly prepared in the flow buffers containing 0−0.5 M NaCl and injected into the flow channel to assess extent of their co-aggregation. As a control to compensate for the nonspecific salt-dependent change in SPR signal caused by different refractivity index values of flow buffers, each flow buffer was injected into the flow channel equilibrated with the flow buffer containing no salt. These background values were then used for background correction.

*Chemical Cross-Linking of Annexin I.* Twenty micrograms (0.5 nmol) of annexin I or its mutants and 0.02 mM of POPC/POPE/POPS (2:5:2 in mole ratio) vesicles (final concentration) were added to 2 mL of 10 mM HEPES-KOH, pH 7.0, containing 0.1 M NaCl and 1 mM Ca$^{2+}$, and the mixture was incubated for 5 min at room temperature. To cross-link the membrane-bound protein, 200 $\mu$L of 10% formaldehyde in phosphate buffer, pH 8.3, was added to the reaction mixture and the mixture was incubated for 30 min. To determine the amount of cross-linked protein, the mixture was centrifuged at 100000$g$ at 25 °C for 20 min using a Sorvall RCM120EX micro-ultracentrifuge. Pellets were redissolved in 15 $\mu$L of 10 mM HEPES-KOH buffer, pH 7.0, containing 100 mM KCl and 1 mM EGTA, and mixed with 15 $\mu$L of the gel-loading buffer (0.125 M Tris-HCl, pH 6.8, 20% (v/v) glycerol, 4% SDS, 0.005% bromophenol blue). These samples were analyzed on 9% SDS−polyacrylamide gels.

## RESULTS

*Models of Annexin I-Induced Membrane Aggregation.* Previous studies on annexin I-induced membrane aggregation indicated the presence of an inducible secondary interaction site for membrane aggregation that is distinct from the primary membrane-binding site (*19*, *28*, *29*, *35*, *36*). Three major topological models of annexin I-mediated membrane aggregation, which are based on the presence of the inducible secondary interaction site, are depicted in Figure 1, panels a−c. Each model could also involve the lateral association of membrane-bound annexin molecules, as shown in Figure 1, panels d−f. The first models assume the direct protein−protein interactions of membrane-bound annexin I molecules (Figure 1, panels a and d), whereas the second ones postulate the interactions of membrane-bound annexin I molecules with the secondary membrane (Figure 1, panels b and e). The third models are different from the second models in that membrane-bound annexin I molecules form axial dimers prior to interacting with the secondary membrane (Figure 1, panels c and f). These models could also be distinguished in terms of different specificity of the secondary interaction site. In the first models, the site would be specific for membrane-bound annexin I, whereas in the second models the site would be specific for the secondary membrane. The third models, on the other hand, would predict that the
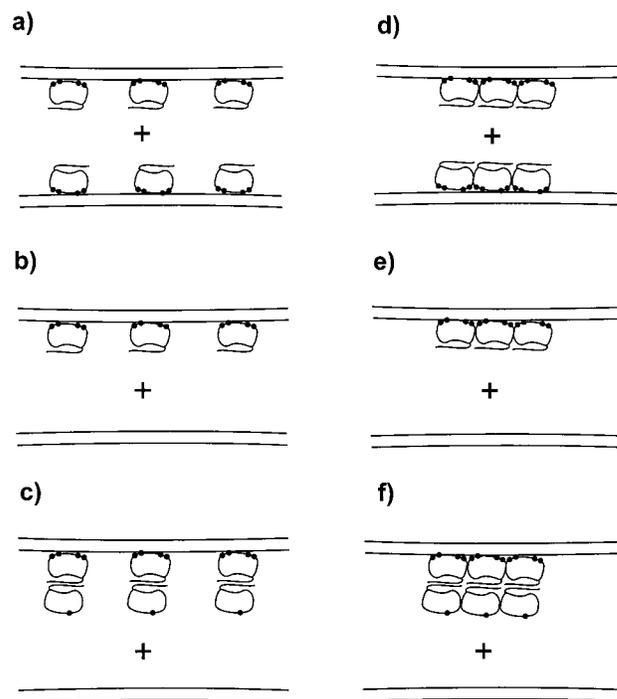


FIGURE 1: Panels a−f: Different models of annexin I-mediated membrane aggregation. See the text for detailed description. Annexin I molecules are shown in a cartoon drawing with its convex side containing multiple calcium binding sites (black dots) facing membranes illustrated in double lines. The concave side of the molecule harbors a flexible amino-terminal region, which forms a part of the secondary interaction site for membrane aggregation.

secondary interaction site is specific for annexin I molecules in solution.

*X-ray Reflectivity Measurements of Annexin-Lipid Monolayer Interactions.* Phospholipid monolayers have been used extensively for the analysis of membrane−annexin interactions (*23*, *31*, *37*−*46*). In particular, this model membrane system allows the separate and independent characterization of primary annexin−membrane interactions, as the secondary membrane for aggregation is not available. To explore the possibility that annexin I binds the lipid monolayer as an axial dimer (or protein bilayer), we analyzed the binding of annexin I to phospholipid monolayers by means of X-ray specular reflection (*32*, *47*, *48*). In this technique, the intensity of X-rays reflected from the air−water interface is measured as a function of $Q_z$, the wave vector transfer (see Materials and Methods) (*32*). As illustrated by eq 1, the X-ray reflectivity represents the Fourier transform of the gradient of the electron density perpendicular to the interface (averaged over the plane of the interface). Analysis of the X-ray reflectivity provides structural information about the monolayer system in the direction perpendicular to the interface.

X-ray reflectivity from the phospholipid monolayer [POPS/POPE/POPC (2:5:2 in mol ratio)] supported on the buffered aqueous subphase is shown in Figure 2, panel a. These data can be fit with a simple two-slab model. The upper slab corresponds to the phospholipid acyl chains, while the lower slab (adjacent to the subphase) corresponds to the phospholipid headgroups. The fitting parameters include the thickness of the two slabs ($L_{acyl}$ = 14 Å and $L_{head}$ = 7 Å), the average electron densities of the two slabs ($\rho_{acyl}$ = 0.8 and $\rho_{head}$ = 1.5, normalized to the value for bulk water, 0.334 $e^-/Å^3$) and the interfacial roughness, $\sigma$ = 4.3 Å, due primarily to
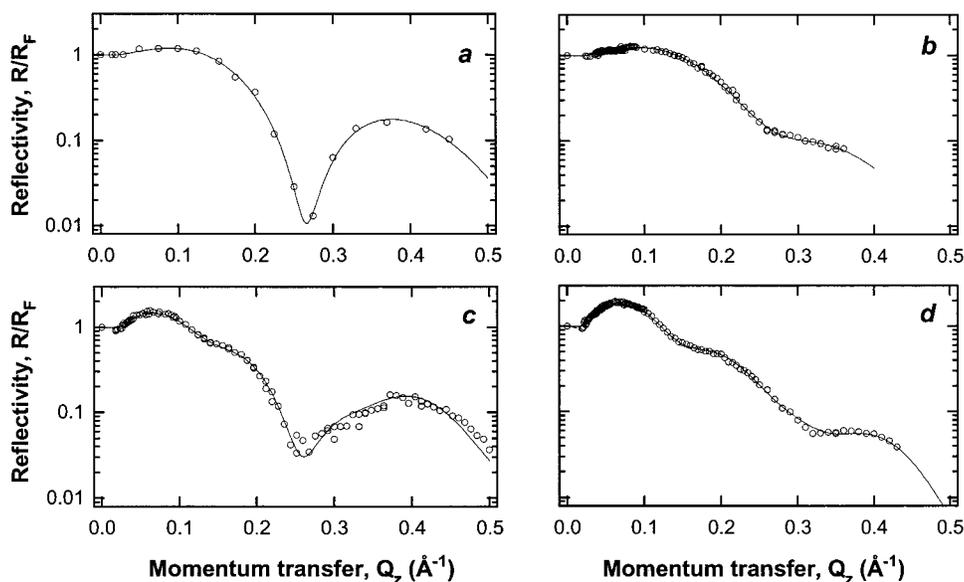
FIGURE 2:  Normalized X-ray reflectivity profiles of phospholipid monolayer-bound annexin I. Phospholipid monolayers, containing POPC/
POPE/POPS (2:5:2), were formed on a subphase buffer (10 mM HEPES-KOH, 0.1 M KCl, pH 7.0), and their surface pressure was set at
34 dyn/cm. The subphase is supplemented with (a) 1 mM $Ca^{2+}$, (b) annexin I (160 $\mu$g), (c) annexin I (160 $\mu$g) and 1 mM $Ca^{2+}$, and (d)
annexin V (500 $\mu$g) and 1 mM $Ca^{2+}$. Open circles indicate experimental data and solid lines represent the best fit of the data using a model
described under Materials and Methods.

capillary waves. The parameters describing the acyl group
region, $L_{acyl}$ and $\rho_{acyl}$, indicate that the acyl chains are
disordered, as expected. The high electron density in the
headgroup region ($\rho_{head} = 1.5$) is due to the presence of
phosphorus and oxygen. The total thickness of the monolayer
adds up to 21 Å, which is consistent with the dimension of
a phospholipid monolayer. These values are in reasonable
agreement with literature values of reflectivity from a pure
DPPC monolayer supported on water (*49*) and other X-ray
measurements of phospholipid assemblies (*50*).

   We then measured the effect of injecting 160 $\mu$g of annexin
I into the subphase containing 1 mM $Ca^{2+}$. The observed
reflectivity (Figure 2, panels c) differed dramatically from
that of the phospholipid monolayer alone. Analysis of the
reflectivity measurements using eq 2 (see Materials and
Methods) indicates the presence of a third slab (due to
annexin I adsorption onto the phospholipid headgroups) with
electron density $\rho_{ann} = 1.11 \pm 0.01$ (relative to water) and
thickness $L_{ann} = (31 \pm 2)$ Å. The parameters describing the
phospholipid monolayer on top of the annexin are very
similar to those discussed above for the monolayer in the
system without annexin. An interfacial profile for the
phospholipid monolayer-bound annexin I is shown in Figure
3 with the roughness set to zero for clarity. These data cannot
be fit with a thickness of $L_{ann} = 62$ Å, indicating that annexin
I adsorbs onto the phospholipids as a monolayer of annexin
I and not as a bilayer. These data thus preclude the possibility
of axial dimer formation of monolayer-bound annexin I
molecules, as illustrated in Figure 1, panels c and f.

   In a control experiment, we injected the same amount of
annexin I into the subphase devoid of free $Ca^{2+}$. The X-ray
reflectivity (Figure 2, panel b) differs slightly from that for
the phospholipid monolayer alone (Figure 2, panel a): a
dampening of the second peak in the reflectivity profile was
seen. Analysis of these control data with a two-slab model
indicates that the headgroup region is thicker than expected
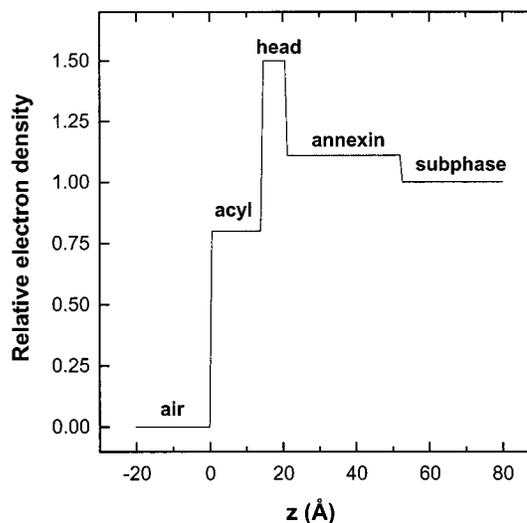(approximately 12 Å, 5 Å larger than expected), which is



FIGURE 3:  Typical interfacial profile of the phospholipid-bound
annexin I. A normalized electron density of the interface along the
axis normal to the interface (*z*) is depicted. Surface roughness
parameter, $\sigma$, was set to zero for clarity.

possibly due to a small amount of denatured annexin I
molecules adsorbed onto phospholipid headgroups. Perhaps
more importantly, the X-ray reflectivity from this control
monolayer without free $Ca^{2+}$ was changing during the 12 h
period of our measurements. During that time, the effective
thickness of the headgroup region increased slightly. All our
other measurements were constant in time, indicating stable
monolayer conformations during similar periods of measure-
ment for either the phospholipids alone or with Annexin (I
or V) with free $Ca^{2+}$. Thus, the formation of the third layer
in Figure 2, panel c, is due to specific, $Ca^{2+}$-dependent
annexin I–phospholipid binding, establishing that the layer
is composed of annexin I molecules adsorbed to phospholipid
monolayer. Most importantly, the thickness of the annexin
layer ($31 \pm 2$ Å) compares well with the molecular
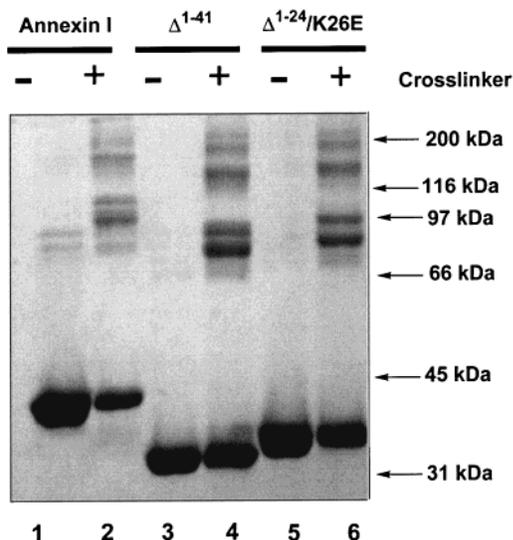dimension of annexin I determined by the X-ray crystal-

FIGURE 4: Chemical cross-linking of membrane-bound annexin I and its truncated mutants. Twenty micrograms of annexin I (lanes 1 and 2), $\Delta^{1-41}$ (lanes 3 and 4), and $\Delta^{1-24}$/K26E (lanes 5 and 6) were incubated with 0.02 mM POPC/POPE/POPS (2:5:2 in mole ratio) vesicles in 10 mM HEPES-KOH, pH 7.0, containing 0.1 M NaCl and 1 mM $Ca^{2+}$ for 5 min before adding formaldehyde (1% final concentration). Samples were incubated for 30 min at 25 °C and centrifuged, and pellets were analyzed on a 9% polyacrylamide gel.

lography, indicating that the protein layer is one molecule thick (*51*).

To verify the validity of our X-ray reflectivity analysis, we also determined the thickness of annexin V molecules bound to the same phospholipid monolayer, which was previously determined by electron and atomic force microscopic analyses (*23*, *52*). X-ray reflectivity measurements resulting from 500 $\mu$g of annexin V injected into the subphase containing 1 mM $Ca^{2+}$ are shown in Figure 2, panel d. The data analysis was again consistent with the presence of three slabs. The third slab (the annexin V) had an electron density $\rho_{ann} = 1.20 \pm 0.01$ (relative to water) and thickness $L_{ann} = 30 \pm 2$ Å. The electron density of this slab is slightly higher than that of annexin I because the coverage of phospholipid monolayer with protein molecules would be higher due to a 3-fold excess of annexin V used in the measurement. Importantly, the calculated thickness of $30 \pm 2$ Å of monolayer-bound annexin V is consistent with the previous values of 22−38 Å and $26 \pm 2$ Å determined by electron and atomic force microscopy, respectively (*23*, *52*). The value also agrees with the dimension of a single annexin V molecule (*20*).

*Cross-Linking of Membrane-Bound Annexin I.* The lateral association and/or two-dimensional crystal formation of membrane-bound annexins has been reported for several annexins, including annexin IV, V, VI, and XII (*23*, *37*−*39*, *52*−*56*). We measured the potential lateral aggregation of membrane-bound annexin I molecules by chemical cross-linking with formaldehyde. A representative electrophero-gram for cross-linked annexin I and its mutants is shown in Figure 4. The cross-linking of annexin I resulted in a large array of high molecular weight aggregates (lane 2), which were absent in the control mixture devoid of the cross-linker (lane 1). Similar patterns were observed with the core of annexin I lacking amino-terminal 41 residues ($\Delta^{1-41}$) that

has limited ability to aggregate phospholipid membranes, and another truncated mutant ($\Delta^{1-24}$/K26E) that has no detectable membrane aggregation activity despite full binding activity (*29*). Differences in electrophoretic mobility of annexin I, $\Delta^{1-41}$, and $\Delta^{1-24}$/K26E and their corresponding aggregates reflect difference sizes of these proteins. Higher molecular weight bands of annexin I and mutants do not exactly correspond to dimers and trimers. This might be because the cross-linked proteins were not fully unfolded in the SDS solution due to the high extent of intra- and intermolecular cross-linking. Note that significant amounts of these proteins remain as a monomer under our conditions, presumably due to incomplete cross-linking reaction. Since our cross-linking was performed under the conditions in which annexin I induces vesicle aggregation, the cross-linked aggregates could derive from either lateral association (Figure 1, panels d and e) or axial association (Figure 1f). Under these conditions, however, $\Delta^{1-24}$/K26E lacking membrane aggregation activity can form only the lateral aggregates, if any. Thus, the finding that annexin I and the two truncated mutants form essentially the same types of cross-linked aggregates indicate that the lateral protein association is mainly responsible for cross-linking and also that the lateral protein association of membrane-bound annexin I is mediated by the carboxy-terminal core.

*Specificity of the Secondary Interaction Site.* A major obstacle in characterizing the secondary interaction site of annexin I is to separate the events of primary and secondary membrane binding, which is difficult to achieve in vesicle-based assays (*28*, *35*). To overcome the difficulty, we employed the surface plasmon resonance technique (*57*, *58*) in which the binding of annexin I to phospholipid vesicles anchored to a sensor chip, and the subsequent binding of vesicles to the membrane-bound annexin I can be separately monitored. In our typical experiment, the dextran-based Pioneer L1 chip that contains multiple hydrophobic anchors was coated with POPS/POPC/POPE (2:5:2 in mole ratio) vesicles and protein solutions were injected into the flow channel of the instrument for primary annexin I-vesicle binding, which was followed by the second injection of the same vesicles for secondary membrane binding and mem-brane aggregation. According to models 1b and 1e (see Figure 1), surface-bound annexin I should be capable of binding the secondary vesicles. Models 1a and 1d, however, predict that surface-bound annexin I cannot bind the second-ary vesicles unless they are precoated with annexin I molecules.

The surface plasmon resonance signal is linearly propor-tional to the mass of analytes interacting with the chip surface (*59*). As shown in Figure 5, the primary membrane binding of annexin to the POPS/POPC/POPE vesicle-coated sensor chip resulted in a large increase of SPR signal. In contrast, annexin I caused a negligible change in SPR signal when the sensor chip was coated with POPC vesicles, demonstrat-ing that the signal increase was due to the specific annexin I-phospholipid binding. The primary binding was $Ca^{2+}$-dependent and reversible, as the injection of $Ca^{2+}$-free buffer rapidly dropped the SPR signal to baseline. Also, dissociation rates of all chip surface-bound proteins used in this study were unusually slow in the flow buffer containing 1 mM $Ca^{2+}$ and 0.1 M NaCl, allowing ready measurement of the secondary binding without having to deal with the loss of
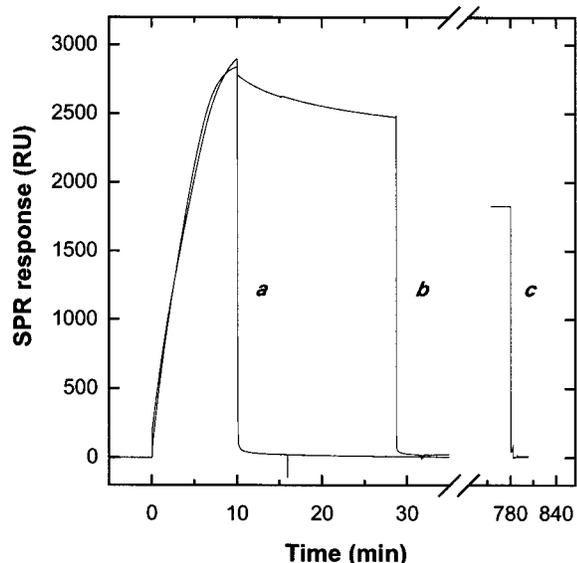
FIGURE 5: Binding of annexin I to vesicle-coated Pioneer L1 sensor chip. The chip was coated with phospholipid vesicles [POPC/POPE/POPS (2:5:2 in mole ratio)] and equilibrated in the flow buffer (10 mM HEPES-KOH, 0.1 M NaCl, pH 7.0) containing 1 mM $Ca^{2+}$. At time zero, 0.1 $\mu$M annexin I solution in the flow buffer containing 1 mM $Ca^{2+}$ was injected at a flow-rate of 10 $\mu$L/min into the flow channel and association was followed for 10 min. At 10 min, injection of protein was stopped, and flow channels were flushed continuously with the flow buffer containing either no $Ca^{2+}$ (a) or 1 mM $Ca^{2+}$ (b or c). Annexin I dissociated very slowly from the chip when the flow buffer contained 1 mM $Ca^{2+}$. Reversibility of the annexin I binding to the chip was demonstrated by the injection of the flow buffer containing no $Ca^{2+}$ at 29.7 min (b) and 780 min (c).
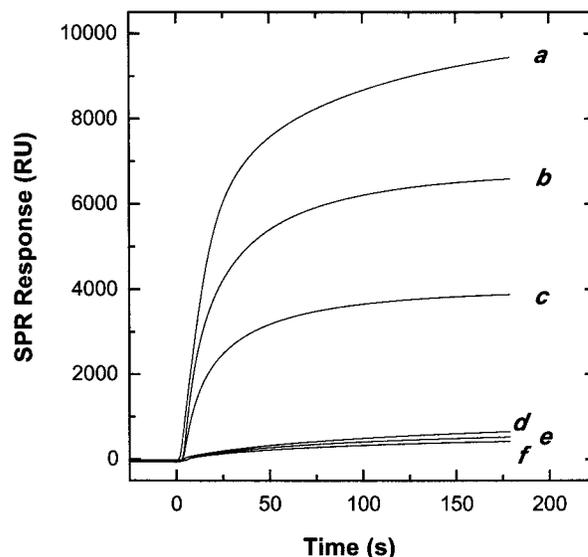


FIGURE 6: Binding of secondary phospholipid vesicles to annexins adsorbed to primary vesicles coated on the Pioneer L1 sensor chip. Proteins analyzed were annexin I (a–b), $\Delta^{1-41}$ (c), $\Delta^{1-24}$/K26E (d) and annexin V (e). Comparable amounts of annexins (2500 RU) were adsorbed to the sensor chip coated with POPS/POPC/POPE (2:5:2 in mole ratio) vesicles. At time zero, 30 $\mu$L of 0.5 mM POPS/POPC/POPE (2:5:2) or POPC (curve b) vesicle solution was injected, and the time course of resonance response was followed for 3 min at 25 °C with a BIACORE X instrument. The flow buffer was 10 mM HEPES-KOH, pH 7.0, containing 0.1 M NaCl and 1 mM $Ca^{2+}$. In a control experiment, the second 30 $\mu$L of 0.5 mM POPS/POPC/POPE (2:5:2) vesicle solution was injected to the sensor chip coated with the same vesicles in the absence of annexins (curve f).

surface-bound protein during the process. For instance, the dissociation of surface-bound annexin I was negligible in typical 6-min-long measurements, and more than 60% of annexin I remained bound to the chip surface even after 13 h (see Figure 5). Primary binding of the same concentration of annexin I, $\Delta^{1-41}$, $\Delta^{1-24}$/K26E, and annexin V all gave comparable increases in SPR signal under the same conditions (data not shown), indicating comparable degree of binding. The sensorgrams depicting the kinetics of secondary membrane binding of surface-bound annexin I and other proteins are shown in Figure 6. Note that the baselines before the vesicle injection are adjusted to zero RU for better illustration. Most significantly, a large increase in SPR signal was observed when POPS/POPC/POPE (2:5:2) vesicles were injected to surface-bound annexin I, suggesting that chip surface-bound annexin I can directly interact with the secondary membrane. Unlike the primary binding, the secondary binding did not have strict requirement for anionic phospholipids, since pure POPC vesicles yielded ≈70% of the signal produced by POPS/POPC/POPE (2:5:2) vesicles (Figure 6, panel b). These signals should arise from the specific adsorption of vesicles to the surface-bound annexin I, as annexin V and $\Delta^{1-24}$/K26E, both of which lack membrane aggregation activity (29), led to negligible increases in SPR signal (Figure 6, panels d and e). Small increases in signal were due to nonspecific interactions of vesicle with the sensor chip because a similar signal was detected when the vesicles were injected into the system with no surface-bound annexins (Figure 6, panel f). To further verify that the observed signal is due to specific secondary membrane binding, we measured the signal with the surface-

bound $\Delta^{1-41}$ (annexin I core), which retains full membrane-binding activity with limited membrane aggregation activity (29). As expected, $\Delta^{1-41}$ caused an intermediate increase in SPR signal upon phospholipid vesicle injection (Figure 6). Overall, these results show that membrane-bound annexin I molecules can directly interact with the secondary membrane, via its specific secondary interaction site, thereby favoring models 1b and 1e over model 1a and 1d (see Figure 1).

*Hydrophobic Nature of Secondary Annexin I-Membrane Interactions.* The primary membrane binding of annexin I is driven by $Ca^{2+}$-dependent electrostatic interactions, which entails the presence of anionic phospholipids in the membrane. Apparent lack of anionic phospholipid requirement for the secondary membrane binding of annexin I suggested that the binding is driven primarily by hydrophobic interactions. To explore this possibility, we determined the salt dependence of the secondary membrane binding by SPR measurements. These measurements were initially hampered by weaker primary binding of annexin I in the presence of high concentrations of NaCl. In particular, lower degree of association and faster off-rates were observed. To overcome this problem, the binding of the annexin I was performed in the flow buffer without NaCl to achieve the high degree of primary binding and the secondary vesicles were prepared in the flow buffers containing different concentrations of NaCl and injected to the chamber. As shown in Figure 7, the binding of surface-bound annexin I to secondary vesicles was further stimulated with the increase in NaCl concentration. The SPR signal in the presence of 0.5 M NaCl was 7 times higher than that seen in the absence of NaCl. This value represented a lower estimate taking into the account
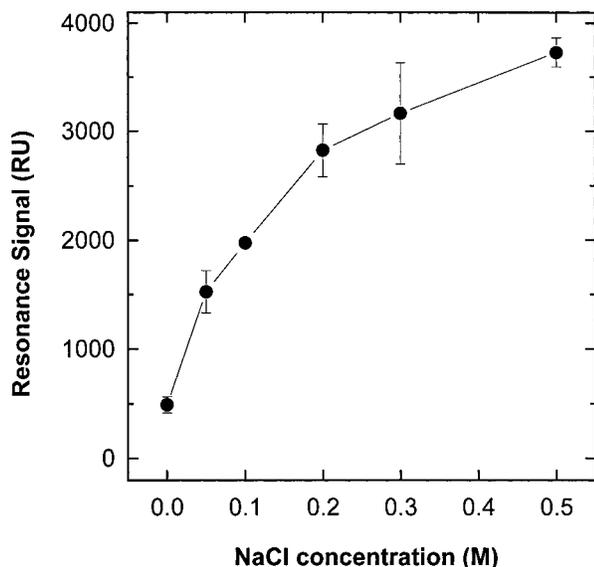
FIGURE 7: Salt dependence of secondary annexin I-vesicle binding. To annexin I molecules (corresponding to 210 RU) bound to the sensor chip coated with POPS/POPC/POPE (2:5:2 in mole ratio), 30 $\mu$L of 0.5 mM POPS/POPC/POPE (2:5:2) vesicle solutions in the flow buffer (10 mM HEPES-KOH, pH 7.0, 1 mM $Ca^{2+}$ and different NaCl concentrations) were injected. The time course of resonance response was followed for 3 min at 25 °C with a BIACORE X instrument, and the final values were taken for plotting. Data points represent means of triplicate determinations and the bars represent standard errors.

the increased protein dissociation rate in the presence of higher concentrations of salt. Overall, these results support the notion that the secondary membrane binding of annexin I is mainly driven by hydrophobic interactions.

## DISCUSSION

Annexin I, as well as annexins II, IV, and VII, have in vitro membrane-aggregation activity (*3, 17*). The membrane-aggregation activity of annexin I can be modulated by phosphorylation and/or proteolysis of amino-terminal region (*29, 35, 60−64*). Also, the activity can be inhibited by annexin I-specific antibodies, independently of its membrane-binding activity (*35, 60*), suggesting the presence of a specific, distinct site for membrane aggregation. Despite extensive efforts, however, the identification of such site has remained elusive. Our recent study indicated that both the core region and some residues in the amino-terminal region, including Lys-26 and Lys-29, are involved in the induction and stabilization of the secondary interaction site (*29*). The present study was undertaken to distinguish whether the secondary site interacts directly with membrane phospholipids or with another annexin I molecule bound to the opposing membrane. To this end, we took an approach of systematic elimination starting from well-defined, comprehensive topological models of annexin I-mediated membrane aggregation (Figure 1), based on two novel biophysical techniques and chemical cross-linking.

An earlier electron microscopic analysis indicated that phospholipid monolayer-bound annexin V molecules form a protein monolayer underneath the lipid monolayer (*23*). However, no such measurement has been reported for annexin I. Our X-ray reflectivity measurements clearly indicate that annexin I (and annexin V) binds to the

phospholipid monolayer as either a monomer or a monolayer. If the annexin I molecule binds to the membrane in an orientation that allows its convex side to make immediate contact with the membrane, the thickness of molecule is estimated to be ≈30 Å from its X-ray structure (*51*). Thus, the calculated thickness of monolayer-bound annexin I (31 ± 2 Å) matches the dimension of a single annexin I molecule. The validity of our methodology was verified by the good agreement between the calculated thickness of annexin V (30 ± 2 Å) monolayer and reported values (22−38 Å and 26 ± 2 Å) (*23, 52*). Also, the calculated thickness of phospholipid monolayer (21 Å) compares well with reported molecular dimension of phospholipids. Although one cannot rule out the possibility that annexin I binds phospholipid monolayers and bilayers in different modes, these data essentially preclude the models involving the axial dimer formation (Figure 1, panels c and f) during the annexin I-induced membrane aggregation.

The two-dimensional crystal formation of phospholipid monolayer-bound annexins has been detected by electron microscopy for several annexins, including annexin IV, V, and VI (*23, 37−39*). The lateral protein crystallization of annexin V bound to the supported bilayer was also demonstrated by atomic force microscopy (*52*). Furthermore, the association of vesicle-bound annexins has been shown by chemical cross-linking, fluorescence, and electron spin resonance. In particular, annexins IV, V, and XII were found to trimerize on the membrane surface (*53−56*). Our chemical cross-linking studies show that annexin I molecules aggregate on the vesicle surface. The association of vesicle-bound annexin I is more likely to occur laterally than axially, as two truncated mutants of annexin I with limited and no membrane aggregation activity, respectively, have essentially the same cross-linking patterns. This also indicates that the lateral protein aggregation is mediated by the core of annexin I, which might be necessary but not sufficient for membrane aggregation activity. Together, our cross-linking studies suggest that membrane-bound annexin I molecules are more likely to function as a protein monolayer than as a monomer, thereby favoring models 1d and 1e over models 1a and 1b.

Finally, we addressed the critical question as to the specificity of the secondary interaction site by means of surface plasmon resonance technology. The main advantage of this system is that it allows separate and independent measurements of primary membrane binding and secondary membrane aggregation events. This was also made possible by the slow dissociation of annexin I from the chip-anchored vesicles, which might be in part due to the stabilization of vesicle-bound annexin I molecules through self-association. In agreement with their reported vesicle-binding activities (*29*), annexin I, its truncated mutants, and annexin V all rapidly bind to the chip-anchored anionic vesicles via calcium-dependent electrostatic interactions. Most importantly, vesicle-bound annexin I yielded a large increase in SPR signal in response to the injection of the secondary vesicles, indicating that it can directly interact with the secondary vesicles. The excellent correlation between the relative membrane-aggregation activity of annexins and the relative SPR signal they produce in response to the secondary vesicle injection supports the notion that the SPR signals directly reflect the secondary membrane binding. Clearly, the secondary membrane binding is mediated not by the

primary membrane binding site but by a distinct site induced by primary vesicle binding, as pure POPC vesicles and anionic POPC/POPE/POPS (2:5:2 in mole ratio) vesicles resulted in comparable SPR signals. The hydrophobic nature of the secondary membrane interactions, as witnessed by our salt dependence study, is also consistent with this notion. Given that the primary membrane binding is inhibited by high ionic strength of medium and the exposure of hydrophobic residues in solution would lead to protein aggregation and precipitation, the hydrophobic secondary interaction site should be induced only after primary membrane binding. A similar observation was reported in an ellipsometric study of annexin I−V chimera in which the chimera could bind pure PC vesicles when adhered to the surface of supported bilayer (*19*). Taken together, our SPR studies indicate that annexin I-induced membrane aggregation is explained best by the model 1e.

On the basis of our previous and present studies, we propose the mechanism by which annexin I induces membrane aggregation. In this mechanism, annexin I first binds the anionic membrane in a calcium-dependent manner. This binding is mediated by the primary membrane binding site located on the convex side of molecule and driven primarily by electrostatic interactions. Once membrane-bound, annexin I molecules undergo subtle conformational changes, which lead to the formation of lateral protein aggregates and the exposure of hydrophobic residues. It appears that the carboxy-terminal core of annexin I is mainly responsible for the protein association, and the amino terminal residues are involved in the induction and stabilization of the hydrophobic secondary binding site. The membrane-bound annexin I molecules directly interact with the secondary membranes mainly via hydrophobic interactions, thereby achieving membrane aggregation. Although this mechanism accounts for much of membrane aggregation by annexin I under our experimental conditions, it remains to be seen whether annexins (other annexins in particular) under different conditions induce the membrane aggregation by the same mechanism. In this regard, it should be noted that electron microscopic analysis provided strong evidence for protein−protein interactions between annexin molecules (annexin I and II) bound to opposite membranes (model 1a and 1d) (*18*). Further studies are needed for comprehensive understanding of mechanisms whereby annexins induce membrane aggregation.

## REFERENCES

1. Raynal, P., and Pollard, H. B. (1994) *Biochim. Biophys. Acta 1197*, 63−93.
2. Swairjo, M. A., and Seaton, B. A. (1994) *Annu. Rev. Biophys. Biomol. Struct. 23*, 193-213.
3. Gerke, V., and Moss, S. E. (1997) *Biochim. Biophys. Acta 1357*, 129−154.
4. Mollenhauer, J. (1997) *Cell Mol. Life Sci. 53*, 506−507.
5. Liemann, S., and Huber, R. (1997) *Cell Mol. Life Sci. 53*, 516−521.
6. Pepinsky, R. B., Tizard, R., Mattaliano, R. J., Sinclair, L. K., Miller, G. T., Browning, J. L., Chow, E. P., Burne, C., Huang, K. S., and Pratt, D. (1988) *J. Biol. Chem. 263*, 10799−10811.
7. Donnelly, S. R., and Moss, S. E. (1997) *Cell Mol. Life Sci. 53*, 533−538.
8. Reutelingsperger, C. P., and van Heerde, W. L. (1997) *Cell Mol. Life Sci. 53*, 527−532.
9. Hajjar, K. A., and Krishnan, S. (1999) *Trends Cardiovasc. Med. 9*, 128−138.
10. Kirsch, T., Nah, H. D., Shapiro, I. M., and Pacifici, M. (1997) *J. Cell Biol. 137*, 1149−1160.
11. von der Mark, K., and Mollenhauer, J. (1997) *Cell Mol. Life Sci. 53*, 539−545.
12. Dubois, T., Oudinet, J. P., Mira, J. P., and Russo-Marie, F. (1996) *Biochim. Biophys. Acta 1313*, 290−294.
13. Alldridge, L. C., Harris, H. J., Plevin, R., Hannon, R., and Bryant, C. E. (1999) *J. Biol. Chem. 274*, 37620−37628.
14. Song, G., Campos, B., Wagoner, L. E., Dedman, J. R., and Walsh, R. A. (1998) *J. Mol Cell Cardiol. 30*, 443−451.
15. Doring, V., Veretout, F., Albrecht, R., Muhlbauer, B., Schlatterer, C., Schleicher, M., and Noegel, A. A. (1995) *J. Cell Sci. 108*, 2065−2076.
16. Buckingham, J. C., and Flower, R. J. (1997) *Mol. Med. Today 3*, 296−302.
17. Creutz, C. E. (1992) *Science 258*, 924−931.
18. Lambert, O., Gerke, V., Bader, M. F., Porte, F., and Brisson, A. (1997) *J. Mol. Biol. 272*, 42−55.
19. Andree, H. A., Willems, G. M., Hauptmann, R., Maurer-Fogy, I., Stuart, M. C., Hermens, W. T., Frederik, P. M., and Reutelingsperger, C. P. (1993) *Biochemistry 32*, 4634−4640.
20. Huber, R., Romisch, J., and Paques, E. P. (1990) *EMBO J. 9*, 3867−3874.
21. Huber, R., Schneider, M., Mayr, I., Romisch, J., and Paques, E. P. (1990) *FEBS Lett. 275*, 15−21.
22. Swairjo, M. A., Concha, N. O., Kaetzel, M. A., Dedman, J. R., and Seaton, B. A. (1995) *Nat. Struct. Biol. 2*, 968−974.
23. Voges, D., Berendes, R., Burger, A., Demange, P., Baumeister, W., and Huber, R. (1994) *J. Mol. Biol. 238*, 199−213.
24. Bitto, E., and Cho, W. (1998) *Biochemistry 37*, 10231−10237.
25. Jost, M., Thiel, C., Weber, K., and Gerke, V. (1992) *Eur. J. Biochem. 207*, 923−930.
26. Jost, M., Weber, K., and Gerke, V. (1994) *Biochem. J. 298 Pt 3*, 553−559.
27. Nelson, M. R., and Creutz, C. E. (1995) *Biochemistry 34*, 3121−3132.
28. de la Fuente, M., and Parra, A. V. (1995) *Biochemistry 34*, 10393−10399.
29. Bitto, E., and Cho, W. (1999) *Biochemistry 38*, 14094−14100.
30. Meers, P., Bentz, J., Alford, D., Nir, S., Papahadjopoulos, D., and Hong, K. (1988) *Biochemistry 27*, 4430−4439.
31. Mukhopadhyay, S., and Cho, W. (1996) *Biochim. Biophys. Acta 1279*, 58−62.
32. Schlossman, M. L., Synal, D., Guan, Y., Meron, M., Shea-McCarthy, G., Huang, Z., Acero, A., Williams, S. M., Rice, S. A., and Viccaro, P. J. (1997) *Rev. Sci. Instrum. 68*, 4372.
33. Born, M., and Wolf, E. (1980) *Principles of Optics*, 6th ed., Pergamon Press, Oxford.
34. Pershan, P. S. (1990) *Faraday Discuss. Chem. Soc. 89*, 231.
35. Meers, P., Mealy, T., Pavlotsky, N., and Tauber, A. I. (1992) *Biochemistry 31*, 6372−6382.
36. de la Fuente, M., and Ossa, C. G. (1997) *Biophys. J. 72*, 383−387.
37. Newman, R., Tucker, A., Ferguson, C., Tsernoglou, D., Leonard, K., and Crumpton, M. J. (1989) *J. Mol. Biol. 206*, 213-219.
38. Newman, R. H., Leonard, K., and Crumpton, M. J. (1991) *FEBS Lett. 279*, 21−24.
39. Mosser, G., Ravanat, C., Freyssinet, J. M., and Brisson, A. (1991) *J. Mol. Biol. 217*, 241−245.
40. Berendes, R., Voges, D., Demange, P., Huber, R., and Burger, A. (1993) *Science 262*, 427−430.
41. Benz, J., Bergner, A., Hofmann, A., Demange, P., Gottig, P., Liemann, S., Huber, R., and Voges, D. (1996) *J. Mol. Biol. 260*, 638−643.
42. Wu, F., Gericke, A., Flach, C. R., Mealy, T. R., Seaton, B. A., and Mendelsohn, R. (1998) *Biophys. J. 74*, 3273−3281.
43. Koppenol, S., Tsao, F. H., Yu, H., and Zografi, G. (1998) *Biochim. Biophys. Acta 1369*, 221−232.

44. Wu, F., Flach, C. R., Seaton, B. A., Mealy, T. R., and Mendelsohn, R. (1999) *Biochemistry 38*, 792−799.

45. Silvestro, L., and Axelsen, P. H. (1999) *Biochemistry 38*, 113−121.

46. Rosengarth, A., Wintergalen, A., Galla, H. J., Hinz, H. J., and Gerke, V. (1998) *FEBS Lett. 438*, 279−284.

47. Schlossman, M. L., and Pershan, P. S. (1992) in *Light Scattering by Liquid Surfaces and Complementary Techniques* (Langevin, D., Ed.) pp 365−403, Marcel Dekker Inc., New York.

48. Schlossman, M. L. (1997) in *Encyclopedia of Applied Physics* (Trigg, G. L., Ed.) pp 311−336, VCH Publishers, New York.

49. Helm, C. A., Mohwald, H., Kjaer, K., and Als-Nielsen, J. (1987) *Europhys. Lett. 4*, 697.

50. Small, D. M. (1986) *The Physical Chemistry of Lipids*, Plenum, New York.

51. Weng, X., Luecke, H., Song, I. S., Kang, D. S., Kim, S. H., and Huber, R. (1993) *Protein Sci. 2*, 448−458.

52. Reviakine, I., Bergsma-Schutter, W., and Brisson, A. (1998) *J. Struct. Biol. 121*, 356−361.

53. Concha, N. O., Head, J. F., Kaetzel, M. A., Dedman, J. R., and Seaton, B. A. (1992) *FEBS Lett. 314*, 159−162.

54. Zaks, W. J., and Creutz, C. E. (1991) *Biochemistry 30*, 9607−9615.

55. Mailliard, W. S., Luecke, H., and Haigler, H. T. (1997) *Biochemistry 36*, 9045−9050.

56. Langen, R., Isas, J. M., Luecke, H., Haigler, H. T., and Hubbell, W. L. (1998) *J. Biol. Chem. 273*, 22453−22457.

57. Myszka, D. G. (1997) *Curr. Opin. Biotechnol. 8*, 50−57.

58. Schuck, P. (1997) *Annu. Rev. Biophys. Biomol. Struct. 26*, 541−566.

59. Jonsson, U., Fagerstam, L., Ivarsson, B., Johnsson, B., Karlsson, R., Lundh, K., Lofas, S., Persson, B., Roos, H., Ronnberg, I., and et al. (1991) *Biotechniques 11*, 620−627.

60. Ernst, J. D., Hoye, E., Blackwood, R. A., and Mok, T. L. (1991) *J. Biol. Chem. 266*, 6670−6673.

61. Wang, W., and Creutz, C. E. (1992) *Biochemistry 31*, 9934−9939.

62. Wang, W., and Creutz, C. E. (1994) *Biochemistry 33*, 275−282.

63. Liu, L., Fisher, A. B., and Zimmerman, U. J. (1995) *Biochem. Mol. Biol. Int. 36*, 373−381.

64. Porte, F., de Santa Barbara, P., Phalipou, S., Liautard, J. P., and Widada, J. S. (1996) *Biochim. Biophys. Acta 1293*, 177−184.